Journal of Catalysis 276 (2010) 390–401

Contents lists available at ScienceDirect

Journal of Catalysis

journal homepage: www.elsevier.com/locate/jcat

Study by isotopic gases and *in situ* spectroscopies (DRIFTS, XPS and Raman) of the N_2O decomposition mechanism on Rh/CeO_2 and $Rh/\gamma\text{-}Al_2O_3$ catalysts

S. Parres-Esclapez [a], I. Such-Basañez [b], M.J. Illán-Gómez [a], C. Salinas-Martínez de Lecea [a], A. Bueno-López [a,*]

[a] Inorganic Chemistry Department, University of Alicante, Ap. 99 E-03080, Alicante, Spain
[b] Instrumental Analysis Service, University of Alicante, Ap. 99 E-03080, Alicante, Spain

ARTICLE INFO

Article history:
Received 12 July 2010
Revised 1 October 2010
Accepted 3 October 2010
Available online 9 November 2010

Keywords:
N_2O decomposition
Rh
Ceria support
$\gamma\text{-}Al_2O_3$
Isotopic exchange
Isotope
DRIFTS
Raman spectroscopy
XPS

ABSTRACT

The N_2O decomposition mechanism on Rh/CeO_2 and $Rh/\gamma\text{-}Al_2O_3$ catalysts has been studied by pulses of isotopic N_2O and O_2 together with *in situ* DRIFT, XP and Raman spectroscopies. The higher catalytic activity of Rh/CeO_2 in comparison with $Rh/\gamma\text{-}Al_2O_3$ is related to the Rh–CeO_2 interaction and to the participation of the CeO_2 support in the N_2O decomposition mechanism, $\gamma\text{-}Al_2O_3$ being an inert carrier. Rhodium on $Rh/\gamma\text{-}Al_2O_3$ is reduced to Rh^0 under reaction conditions and N_2O decomposition over this catalyst mainly occurs via the Eley–Rideal mechanism. On the contrary, the ceria support interacts strongly with rhodium partially stabilizing cationic species of the noble metal during N_2O decomposition. In Rh/CeO_2, the reduced rhodium sites (by N_2O) can be reoxidized afterwards either by N_2O or by ceria oxygen, and the vacant sites created on the ceria support are then oxidized by N_2O. The active sites for N_2O chemisorption and decomposition are not only located on rhodium but also on ceria.

1. Introduction

The environmental impact of N_2O has attracted strong attention because of its contribution to global warming and ozone depletion in the upper atmosphere [1]. N_2O is emitted as a by-product in several chemical processes of high industrial relevance, such as nitric acid and adipic acid production. In addition, N_2O emission by vehicles also takes place due to the ageing of the catalytic converters used for NO_x emissions abatement.

The most effective solution to remove N_2O from gas streams is to use catalysts to either promote N_2O decomposition or to facilitate its reaction with a reducing agent. The former process is preferred because additional reactants are not required, and several catalysts have been developed for N_2O decomposition [1].

Several mechanisms have been proposed to describe the catalytic decomposition of N_2O [1–6]. The study of these mechanisms is based, in most cases, on the analysis of the effect of the N_2O partial pressure and temperature on the N_2O decomposition rate. The catalytic N_2O decomposition reaction has been described as a molecular adsorption of N_2O on active sites of the catalyst (∗) followed by the decomposition of the N_2O molecule with N_2 release.

$$* + N_2O \Longleftrightarrow *\text{—}N_2O$$

$$*\text{—}N_2O \rightarrow N_2 + *\text{—}O$$

Transient kinetic studies performed with MnO_2, for instance, demonstrated that not all the adsorption sites suitable for N_2O adsorption are active for N_2O decomposition [7]. On the other hand, depending on the catalyst nature, dissociative chemisorption of N_2O can occur in a single step instead of molecular adsorption followed by surface decomposition:

$$* + N_2O \rightarrow N_2 + *\text{—}O$$

The oxygen atoms left on the active sites (∗–O) can be desorbed by recombination, with O_2 release (Langmuir–Hinshelwood mechanism):

$$2\,*\text{—}O \Longleftrightarrow 2* + O_2$$

or by reaction with another N_2O molecule (Eley–Rideal mechanism):

$$*\text{—}O + N_2O \rightarrow * + N_2 + O_2$$

Note that the recombination of oxygen atoms is a reversible process, while the regeneration of active sites by N_2O is irreversible [4]. The reversibility of the former reaction explains why O_2 has an inhibitory effect on most N_2O decomposition catalysts, since N_2O and O_2 compete for the active sites of the catalyst [4].

* Corresponding author. Address: Ap. 99 E-03080, Alicante, Spain. Fax: +34 965903454.
E-mail address: agus@ua.es (A. Bueno-López).

0021-9517/$ - see front matter © 2010 Elsevier Inc. All rights reserved.
doi:10.1016/j.jcat.2010.10.001

The interaction of the O_2 molecules with catalytic surfaces has been deeply studied [8–13], and the knowledge about these interactions is useful to explain some aspects of the N_2O decomposition mechanism and to develop catalysts for N_2O decomposition in O_2-rich streams. Isotopic gases are very useful to study the interaction of gas molecules with solid catalysts, and many studies have been carried out with $^{18}O_2$ [14,15]. From these studies, it has been concluded that there are three main processes involved in the oxygen exchange mechanisms between molecular oxygen and metal oxide surfaces: the dissociative chemisorption of molecular oxygen, the exchange of atoms or adsorbed ions and desorption of molecular oxygen. The exchange of oxygen atoms can occur in a single step or in two consecutive steps, and the nature of the solid surface significantly affects these processes.

Among the different catalysts studied for N_2O decomposition, Rh catalysts are highly active, and the activity depends on the support used [16,17]. Ceria-based supports, either pure or doped with La or Pr, for instance, enhance the catalytic activity of rhodium with regard to alumina supports. This improvement seems to be related to the redox properties of ceria, and it was suggested that cerium oxide is also involved in N_2O decomposition. However, the reaction mechanism behind such enhanced performance of rhodium when supported on ceria is still unknown.

The interaction of ceria-based oxides with isotopic O_2 has been widely studied [9,18–20], and the oxygen exchange capacity of this type of oxides is extremely high and fast. In some cases, the interaction of ceria-based materials with some other oxygen-containing isotopic gases different to $^{18}O_2$ has been studied. For example, Cunningham et al. [18] studied the exchange of oxygen between $^{15}N^{18}O$ and CeO_2, which takes place from 175 °C, and evidences of the oxygen exchange between $C^{18}O_2$ and CeO_2 have also been reported [21,22]. The oxygen exchange mechanism between isotopic CO_2 and Pt/CeO_2 catalyst occurs in two consecutive steps, and the exchange of both $C^{18}O_2$ oxygen atoms prevails with regard to the single exchange. However, as far as we know, the interaction of isotopic N_2O with Rh/ceria catalysts has not been reported.

The aim of this study is to determine the rhodium-catalysed N_2O decomposition mechanisms, in order to understand the improved activity of Rh/ceria with regard to Rh/alumina catalysts. The approach followed combines pulse experiments of isotopic N_2O and isotopic O_2 with *in situ* XPS, DRIFTS and Raman spectroscopy experiments. The combination of all these techniques provides complementary information about the reaction mechanisms. The experiments with isotopic gases provide information about the participation of catalyst oxygen in the N_2O decomposition mechanism, *in situ* DRIFTS allows monitoring the surface nitrogen groups during the reaction and *in situ* XPS and *in situ* Raman spectroscopy are useful to identify changes in the catalyst during N_2O decomposition, such as changes in the oxidation states of the metals involved in the reaction mechanism.

2. Experimental

2.1. Catalysts preparation

Two powder catalysts have been used in this study, which are referred to as Rh/CeO_2 and $Rh/\gamma\text{-}Al_2O_3$. The CeO_2 support was prepared by $Ce(NO_3)_3{\cdot}6H_2O$ (Aldrich, 99.9%) calcination in static air at 600 °C for 90 min (heating rate 10 °C/min). The $\gamma\text{-}Al_2O_3$ support was prepared from commercial $\gamma\text{-}Al_2O_3$ pellets (Across), which were crushed in a mortar. Rh was loaded on the CeO_2 and $\gamma\text{-}Al_2O_3$ supports (125–200 μm particle size) by incipient wetness impregnation with a water solution of $Rh(NO_3)_3$ (Sigma Aldrich, 99.9%). Finally, both catalysts were dried at 200 °C and calcined at 500 °C for 2 h. The target content of Rh in both catalysts, after calcination, was 0.5 wt.%.

The supports and catalysts were characterized by Raman spectroscopy, XRD, N_2 adsorption at −196 °C, H_2–TPR and TEM, and detailed information about such characterization was reported elsewhere [16]. Briefly, it is important to mention that both supports present similar BET surface area (76 m^2/g CeO_2 and 78 m^2/g $\gamma\text{-}Al_2O_3$) and similar rhodium particle size (average size of rhodium particles 2.2 nm in Rh/CeO_2 and 2.3 nm in $Rh/\gamma\text{-}Al_2O_3$, as observed by TEM).

2.2. N_2O decomposition tests in a fixed-bed reactor

N_2O decomposition tests were performed at atmospheric pressure in a 10-mm i.d. cylindrical fixed-bed reactor, with 100 mg of catalyst diluted with 700 mg of SiC and a total gas flow of 100 ml/min (GHSV = 10,000 h^{-1}). The catalytic bed was packed between plugs of quartz wool. Different N_2O/He mixtures, with N_2O concentrations of 100, 300, 600, 1000 and 1400 ppm were evaluated, and experiments with 1000 ppm N_2O/5% O_2/He were also performed. The gas composition was analysed by a HP 6890 gas chromatograph equipped with a thermal conductivity detector and two serial columns (Porapak Q, for N_2O, and Molecular Sieve 13X, for O_2 and N_2).

The experiments consisted of point-by-point isothermal reactions in the range 200–400 °C, and all reactions were extended to the steady state (typically between 20 and 40 min were needed). A typical experiment consisted of heating the as prepared (fresh) catalyst under the selected gas flow at 200 °C, where N_2O decomposition does not occur in any case. Once all gas concentrations are stable, the temperature is raised 25 °C, and this procedure is repeated to 400 °C. Then, the temperature is lowered to room conditions under He flow, the next gas mixture to be studied is fed to the reactor and the heating steps are repeated as described. All experiments have been carried out with the same sample of each catalyst. In order to ensure that their catalytic activity does not change during the catalytic cycles, catalytic tests under 1000 ppm N_2O/He have been performed as control tests every few catalytic cycles. As will be discussed afterwards, only the $Rh/\gamma\text{-}Al_2O_3$ catalyst showed different catalytic activity during the first and second runs performed (under identical conditions), but not in further cycles where the catalytic activity of the second cycled is maintained.

2.3. XPS characterization after in situ treatments under reaction conditions

XPS experiments were carried out in a VG-Microtech Multilab electron spectrometer using Mg Kα (1253.6 eV) radiation source. To obtain the XPS spectra, the pressure of the analysis chamber was maintained at 5×10^{-10} mbar. The binding energy (BE) and the kinetic energy (KE) scales were adjusted by setting the C1*s* transition at 284.6 eV, and BE and KE values were determined with the software Peak-fit of the spectrometer. XPS spectra of the fresh catalysts Rh/CeO_2 and $Rh/\gamma\text{-}Al_2O_3$ and after 1 h *in situ* treatments under 1000 ppm N_2O/Ar or pure Ar at different temperatures between 250 and 325 °C were recorded. The *in situ* treatments were carried out before the XPS measurement in an auxiliary reaction chamber, where the sample is heated to the selected temperature, and the gas mixture is fed at 1 atm total pressure. After the treatment, the sample was introduced into the XPS chamber avoiding exposure to air, and spectra were recorded at room temperature.

2.4. In situ Raman spectroscopy experiments

Raman spectra were recorded in a multichannel dispersive Raman spectrometer (Labram from Jobin–Yvon Horiba) with a laser source He:Ne (632.8 nm) using a Peltier cooled CCD as a detector.

The spectrometer is coupled to a confocal microscope (confocal hole set to 600 nm). As a monochromator, a diffraction grating of 600 lines/mm with an entrance slit of 200 nm was used providing a spectral resolution of 4 cm^{-1}. Starting with fresh catalyst Rh/CeO_2, *in situ* experiments at different temperatures under 1000 ppm N_2O/Ar flow have been performed in the Raman spectrometer with a Linkam THMS600 reaction cell. Similar experiments under pure Ar flow were performed.

2.5. Pulse experiments with isotopic gases ($^{15}N_2{}^{18}O$ and $^{18}O_2$)

$^{18}O_2$ (Isotec, 99%) and $^{15}N_2{}^{18}O$ (Isotec, min 98% ^{15}N, min 95% ^{18}O) were used in the pulse experiments. The experiments were carried out in a 5-mm i.d cylindrical fixed-bed reactor with 50 mg of catalyst. The fresh catalyst was packed between plugs of quartz wool. The carrier gas used was a 10 ml/min flow of He. The experimental procedure consists of feeding three pulses of the selected gas at each one of the following temperatures: 50, 200, 250, 300, 350 and 400 °C. Once the maximum temperature is reached, the He flow is replaced by air, and the temperature is cooled down to 50 °C. Then air is replaced by He, and the same procedure is repeated with another gas. First, pulse experiments with Ar, N_2O and O_2 (non-isotopic) were carried out consecutively, in order to evaluate the system response. After the non-isotopic pulses, pulses of $^{15}N_2{}^{18}O$ and $^{18}O_2$ were performed.

The experimental set-up used mainly consists of a set of mass flow controllers (0.1 ml/min sensitivity), an injection valve with a 100-μl loop, and two high-sensitivity pressure transducers, which allow the gas injections to be performed without a concomitant pressure variation in the system. A vacuum pump is used to evacuate the helium into the loop and, once empty, a pressure regulator is used to fill up the loop with the isotopic gas at 5 psi. The gas composition was monitored with a mass spectrometer Pfeiffer Vacuum (model OmniStar), operating at 1-s frequency.

2.6. In situ DRIFTS-MS experiments

A FTIR spectrometer (model Infinity MI60 from Mattson) with a diffuse reflectance accessory (model COLLECTOR from Spectra Tech) was used for *in situ* DRIFTS experiments. A reaction cell fitted with $CaCl_2$ windows, which allows temperature and gas flow composition control, was used. The gas composition is monitored during the experiments with a mass spectrometer Pfeiffer Vacuum (model OmniStar).

Before the DRIFTS experiments under N_2O-containing gas mixtures, the catalysts were *in situ* treated at 450 °C under helium flow to remove adsorbed species. Afterwards, the temperature was lowered to room conditions (30 °C), and the inert gas was replaced by a gas mixture of 1000 ppm N_2O/He or 1000 ppm N_2O/5% O_2/He. The temperature is raised in steps of 25 °C, and once the steady state is reached both in the gas composition and in the catalyst surface, the spectrum is recorded at each temperature. The background spectra were recorded for each catalyst at room temperature under He flow, and therefore carbonate bands and some other catalyst features do not appear in the spectra recorder under reaction conditions. Spectra were recorded with a resolution of 2 cm^{-1}.

3. Results

3.1. N_2O decomposition tests

Fig. 1 presents the N_2O decomposition rates as a function of temperature obtained with the catalysts Rh/γ-Al_2O_3 (Fig. 1a) and Rh/CeO_2 (Fig. 1b) during the first and second runs, which were performed under 1000 ppm N_2O/He, and during the third run, which was performed under 1000 ppm N_2O/5% O_2/He. The N_2O decomposition rates on the CeO_2 and γ-Al_2O_3 supports, also included in Fig. 1, are negligible under the reaction conditions of these experiments. The rates affected by mass transfer effects (dashed lines) are distinguished from those measured under chemical control (continuous lines).

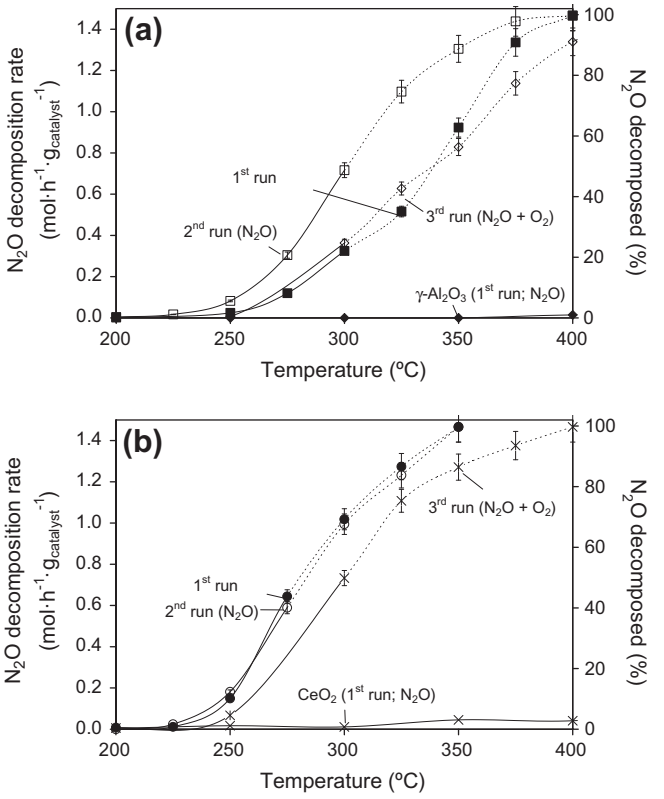

Fig. 1. N_2O decomposition rates and conversions as a function of temperature in tests conducted with 1000 ppm N_2O/He (1st and 2nd runs) or with 1000 ppm N_2O/5% O_2/He (3rd run). (a) Rh/Al_2O_3 and (b) Rh/CeO_2 (continuous lines: data obtained under chemical control of the reaction rate. Dashed lines: data affected by mass diffusion).

For experiments conducted under equal conditions, the N_2O decomposition rate on the Rh/γ-Al_2O_3 catalyst (Fig. 1a) is lower than that on Rh/CeO_2 (Fig. 1b). The N_2O decomposition rates measured with Rh/CeO_2 during the first and second cycle are equal, while the decomposition rates of Rh/γ-Al_2O_3 increase after the first run. This activation process will be studied and discussed in the coming sections. As expected, the N_2O decomposition rates decrease partially in the presence of O_2 (3rd run). This decrease is reversible, that is, the N_2O decomposition rate increases to the original level if O_2 is removed from the gas stream. It has been reported [1] that O_2 inhibits partially the catalytic activity of most N_2O decomposition catalysts, in a different extent depending on the nature of the catalyst, due to O_2 chemisorption on the catalyst active sites.

The N_2O decomposition rates measured with our catalysts, under chemical control of the reaction rate, are higher than some values reported by other authors. For instance, the N_2O decomposition rates of our catalysts under 1000 ppm N_2O + 5%O_2 at 300 °C are 0.36 and 0.71 $mol(N_2O)\cdot g^{-1}\,h^{-1}$ for Rh/γ-Al_2O_3 and Rh/CeO_2, respectively. Comparatively, it has been reported [23] a N_2O decomposition rate of 0.37 $mol(N_2O)\cdot g^{-1}\,h^{-1}$ for a 0.5 wt.%Rh/CeO_2 catalyst measured under a gas mixture with 950 ppm N_2O + 5%O_2 at 400 °C. The lower rate obtained with this Rh/CeO_2 catalyst [23] in comparison with our results could be attributed to the low surface area of the catalyst tested (9 m^2/g) with regard

to the surface area of our samples (76–78 m^2/g). The N_2O decomposition rates of our catalysts are also higher than values reported for other Rh/CeO_2 and Rh/Al_2O_3 catalysts [24] (with 22 and 168 m^2/g, respectively, and both with 2 wt.%Rh). This comparison evidences that the catalytic activity for N_2O decomposition of the Rh catalysts not only depends on the nature of the active phases but also on the particular physicochemical features of each catalyst.

N_2O decomposition experiments were performed with the Rh/CeO_2 and $Rh/\gamma\text{-}Al_2O_3$ catalysts under N_2O/He gas streams with different N_2O partial pressures in the range 100–1400 ppm. The results obtained were fitted with n-order kinetic equations and the apparent reaction orders towards N_2O, and the reaction constants at each temperature were estimated from these calculations. Fig. 1SM in supplementary material shows the experimental rates and the corresponding model fittings, from which the reaction constant and apparent N_2O reaction orders were estimated. Once the reaction constants were determined, Arrhenius-type plots (Fig. 2SM in supplementary material) were used to determine the apparent activation energies.

The kinetic data obtained are compiled in Table 1. The apparent N_2O reaction orders are quite similar for both catalysts, and the values obtained are lower than 1. This means that the N_2O decomposition rates are not linearly proportional to the N_2O partial pressure. The decomposition rate is faster in concentrated streams than in those diluted, which has important relevance for practical applications. Kapteijn et al. [1] compiled the information available in the literature about the catalytic decomposition of N_2O using a wide variety of materials including pure metals and metal oxides, spinel-type mixed oxides, perovskites and hydrotalcites, zeolites and metals and transition metal oxides supported on alumina, silica and zirconia. In all cases, it was founded that the apparent reaction order with respect to the N_2O partial pressure is 1 or slightly lower, suggesting that values below 1 may be related to the inhibitory effect of O_2 formed as reaction product. This argument seems also valid for the catalysts studied in this article.

The apparent activation energies estimated, listed in Table 1, were different for $Rh/\gamma\text{-}Al_2O_3$ and Rh/CeO_2 (146 and 121 kJ/mol, respectively). These values are consistent with activation energies reported in the literature for noble metal and transition metal oxide catalysts (typically between 80 and 170 kJ/mol) [1] and are lower than the energy required to break the N–O bond in the N_2O molecule without catalyst participation (250–270 kJ/mol) [25–28], which requires about 625 °C [29]. The different apparent activation energy obtained with $Rh/\gamma\text{-}Al_2O_3$ and Rh/CeO_2 implies that the N_2O decomposition mechanisms are different on the two catalysts or that there are differences in the rate-limiting step. The reaction mechanisms have been studied in the current article by different techniques, and as will be discussed in coming sections, important differences between $Rh/\gamma\text{-}Al_2O_3$ and Rh/CeO_2 have been noticed.

3.2. XPS characterization

The changes in the oxidation states of Rh and Ce during the catalytic decomposition of N_2O and the Rh/Al and Rh/Ce ratios have been studied by XPS. The fresh Rh/CeO_2 and $Rh/\gamma\text{-}Al_2O_3$ catalysts and also the catalysts after *in situ* treatments with 1000 ppm N_2O/Ar at different temperatures have been characterized by XPS.

Table 1
Apparent N_2O reaction orders and activation energies for Rh/CeO_2 and $Rh/\gamma\text{-}Al_2O_3$ catalysts.

	N_2O reaction order	Activation energy (kJ/mol)
$Rh/\gamma\text{-}Al_2O_3$	0.74 ± 0.03	146 ± 5
Rh/CeO_2	0.68 ± 0.03	121 ± 5

Table 2 compiles the XPS-measured Rh/Al and Rh/Ce atomic surface ratios. Rh/Ce ratios are higher than Rh/Al ratios, regardless of the temperature of the pre-treatment, evidencing that Rh dispersion on ceria is higher than on alumina both in fresh and in used catalysts. This result contrasts with the TEM-estimated rhodium particle sizes because, as mentioned, the average size of rhodium particles is almost equal in both catalysts (2.2 nm in Rh/CeO_2 and 2.3 nm in $Rh/\gamma\text{-}Al_2O_3$ [16]). A detailed analysis of our TEM pictures lead us to think that particles lower than 1 nm are hardly observed in the Rh/CeO_2 catalyst in our TEM device. However, they should exist on Rh/CeO_2 but not on $Rh/\gamma\text{-}Al_2O_3$. It must be taken into account that the molecular weight of cerium is much higher to that of aluminium, and therefore, the Rh–Al colour contrast is much better than the Rh–Ce contrast. This experimental limitation of TEM would overestimate the average particle size of Rh on the Rh/CeO_2 catalysts.

According to data on Table 2, the rhodium particles sinter under reaction conditions between 250 and 275 °C, since the Rh/Al and Rh/Ce atomic ratios decrease above this threshold. However, Rh sintering seems to affect more to $Rh/\gamma\text{-}Al_2O_3$ than to Rh/Ceria, which is in agreement with the well-known stabilizing effect of ceria [30].

Fig. 2 shows XP spectra obtained with $Rh/\gamma\text{-}Al_2O_3$ (Fig. 2a) and Rh/CeO_2 (Fig. 2b) corresponding to the electronic transitions Rh $3d^{3/2}$ and Rh $3d^{5/2}$, with binding energies at 312–315 eV and 306–310 eV, respectively. It has been reported that the Rh $3d^{5/2}$ peaks of CeO_2-supported Rh^0 appear with binding energies in the range 307.0–307.7 eV, while Rh^{3+} species on the same support appear at 308.3–310.5 eV [17,31,32]. For Al_2O_3-supported Rh, it has been reported that the peaks corresponding to Rh^0 are shifted towards lower binding energies in comparison with Rh/CeO_2, appearing at ~306 eV [33]. In our fresh $Rh/\gamma\text{-}Al_2O_3$ and Rh/CeO_2 catalysts, the Rh $3d^{5/2}$ binding energies appear at about 309 eV, evidencing the presence of Rh^{3+} species in both catalysts. This was expected taking into account that the catalysts were calcined in air at 500 °C.

These Rh^{3+} species are partially or totally reduced to Rh^0 during the catalytic decomposition of N_2O, as deduced from Fig. 2, and the support plays a major role in this reduction process. For $Rh/\gamma\text{-}Al_2O_3$ (Fig. 2a), the binding energy of the Rh $3d^{5/2}$ transition decreases from around 309 eV at 275 °C to about 306.4 eV at 300 °C and higher temperature, evidencing the reduction of Rh^{3+} to Rh^0. Note that N_2O decomposition on $Rh/\gamma\text{-}Al_2O_3$ (see Fig. 1, 1st run) is low below 275 °C and increases significantly above this temperature. This would mean that Rh^0 is the most active species of rhodium when supported on alumina, which would also explain the increase in the N_2O decomposition rate during the second run, once Rh^{+3} species are reduced to Rh^0.

On the contrary, the reduction of rhodium under reaction conditions progressively occurs with temperature in the Rh/CeO_2 catalyst (Fig. 2b). In this case, the Rh $3d^{5/2}$ peaks can be deconvoluted into two peaks corresponding to species of Rh^{3+} and Rh^0 (high and low binding energy contributions, respectively). From the area of these deconvoluted peaks, the percentages of Rh^{3+} and Rh^0 have

Table 2
XPS-measured atomic surface ratios in fresh catalysts and after 1 h *in situ* treatments under 1000 ppm N_2O/He at different temperatures.

Temperature (°C)	Rh/Al atomic ratio in $Rh/\gamma\text{-}Al_2O_3$	Rh/Ce atomic ratio in Rh/CeO_2
Fresh catalysts	0.013	0.084
250	0.011	0.099
275	0.006	0.066
300	0.007	0.063
325	0.006	0.056

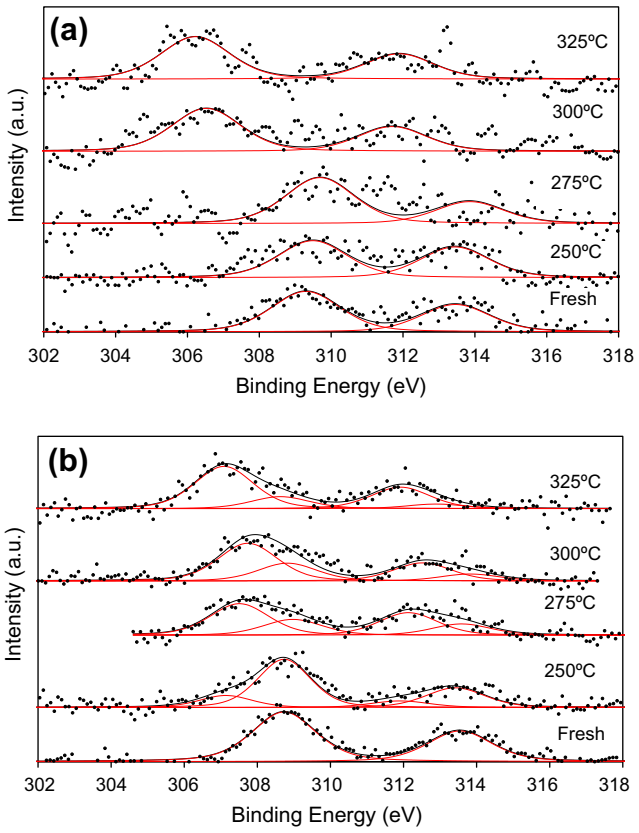

Fig. 2. XPS spectra of the Rh 3d transition for the fresh catalysts and after *in situ* treatments with 1000 ppm N_2O/Ar for 1 h at different temperatures. (a) Rh/γ-Al_2O_3 and (b) Rh/CeO_2.

been estimated, and the results obtained for Rh^0 are compiled in Table 3. These results reveal that part of the Rh^{3+} species on the Rh/CeO_2 catalyst remain oxidized under reaction conditions to 325 °C (at least). According to these XPS results, the ceria support strongly interacts with rhodium and partially stabilizes the cationic species under reaction conditions. This stabilizing effect would explain the equal catalytic results (Fig. 1b) obtained during the first and second cycle of experiments performed with the Rh/CeO_2 catalyst.

The behaviour of the cerium oxidation state under N_2O decomposition conditions has also been studied by XPS with the Rh/CeO_2 catalyst. For comparison, the same *in situ* treatments performed with 1000 ppm N_2O/Ar have been repeated with fresh Rh/CeO_2 catalyst under pure Ar. The Ce 3d core level has been analysed and, after deconvolution of the experimental spectra, the degree of ceria reduction has been calculated from the ratio of the sum of the intensities of the u_0, u_1, v_0 and v_1 bands to the sum of the intensities of all the bands, following the method proposed elsewhere [34]. As example, the Ce 3d photoelectron spectra of Rh/CeO_2 after *in situ* thermal treatments at 325 °C under Ar and N_2O/Ar are included as Supplementary data (Fig. 3SM).

Table 3
XPS-estimated Rh^0 percentage in fresh catalysts and after 1 h *in situ* treatments under 1000 ppm N_2O/He at different temperatures.

Temperature (°C)	Rh/γ-Al_2O_3	Rh/CeO_2
Fresh catalysts	0	0
250	0	20
275	0	66
300	100	68
325	100	78

The Ce^{3+} percentages determined by XPS after *in situ* treatments performed under 1000 ppm N_2O/Ar or pure Ar have been plotted in Fig. 3 as a function of temperature. It is important to mention that ceria can be partially reduced under the high vacuum conditions of the XPS measurements. For this reason, the Ce^{3+} percentages determined by XPS are expected to differ from the real values under reaction conditions in a fixed-bed reactor. However, the differences between the Ce^{3+} trends obtained under Ar and N_2O/Ar provide valuable information about the catalysts behaviour. At 250 °C, where the catalytic activity is very low (see Fig. 1a), the Ce^{3+} percentage is equal (32.7%) after both thermal treatments performed, regardless of the gas used. The Ce^{3+} percentage increases with temperature for experiments performed under pure Ar while it remains almost constant under 1000 ppm N_2O/Ar. This means that the ceria support delivers oxygen during the thermal treatment under inert conditions, while N_2O is able to restore the oxygen balance of ceria by oxidation of the vacant sites created on ceria upon thermal reduction.

3.3. *In situ* Raman spectroscopy characterization of the Rh/CeO_2 catalyst

The Rh/CeO_2 catalyst has been characterized by Raman spectroscopy under reaction conditions. Raman spectra have been recorded at different temperatures under gas streams of pure Ar or 1000 ppm N_2O/Ar. The spectra obtained at 150 and 350 °C are shown in Fig. 4a (Ar) and b (N_2O/Ar), as examples. The main peak at around 460 cm^{-1} is the typical fluorite peak of ceria assigned to the F_{2g} mode. This peak presents a shoulder between 500 and 700 cm^{-1} including contributions of vacant sites of the ceria support and RhO_x species. The small peak at 230 cm^{-1} can be also attributed to RhO_x species, and this peak is only observed in some of the spectra [35–37].

The gas composition used for the thermal treatments significantly affects the changes observed in the Raman spectra of the Rh/CeO_2 catalyst. The RhO_x peak at 230 cm^{-1} decreases at 350 °C under Ar (Fig. 4a) but remains invariable under N_2O/Ar. This indicates that the RhO_x species are thermally unstable under Ar atmosphere, while they are stable in the presence of N_2O. On the other hand, the intensity of the shoulder between 500 and 700 cm^{-1} increases from 150 to 350 °C under Ar (Fig. 4a) due to the creation of vacant sites on ceria, while it slightly decreases under N_2O/Ar, because some vacant sites are depleted by N_2O oxidation. Finally, attention must be paid to the position of the F_{2g} peak. In Fig. 5, the position of the F_{2g} peak for experiments performed under Ar and N_2O/Ar has been plotted versus temperature. Under both gases, the position of the F_{2g} peak decreases with temperature reaching a more or less constant value at 150 °C under N_2O/Ar and at 250 °C on pure Ar. This decrease in the F_{2g} peak position

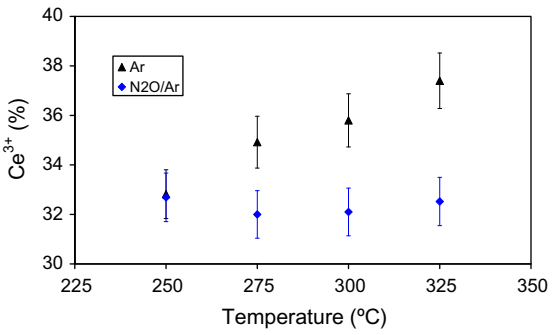

Fig. 3. Ce^{3+} percentage with regard to Ce^{3+} + Ce^{4+} estimated from XPS analysis of the Rh/CeO_2 catalyst after *in situ* treatments with 1000 ppm N_2O/Ar or pure Ar for 1 h at different temperatures.

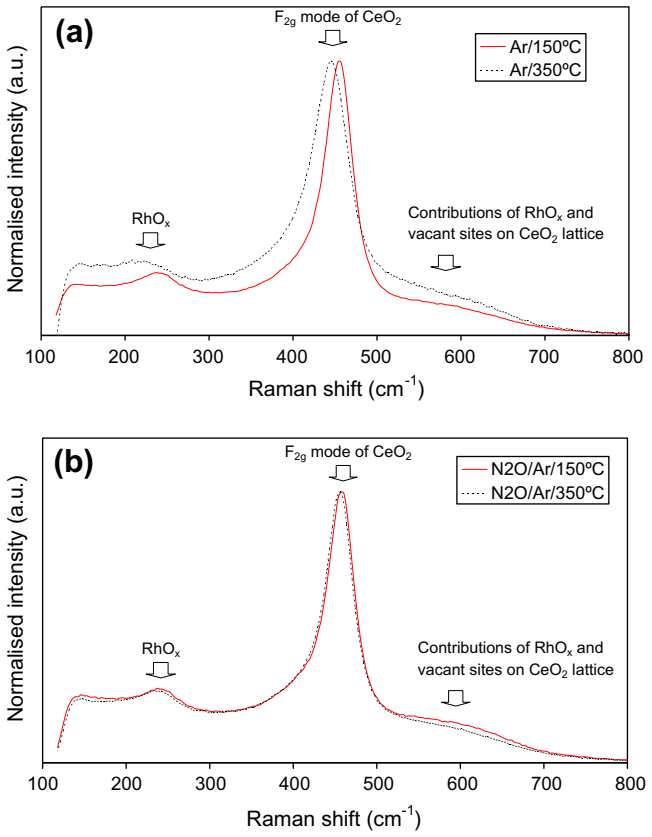

Fig. 4. Raman spectra of the Rh/CeO_2 catalyst obtained at different temperatures under (a) Ar and (b) 1000 ppm N_2O/Ar.

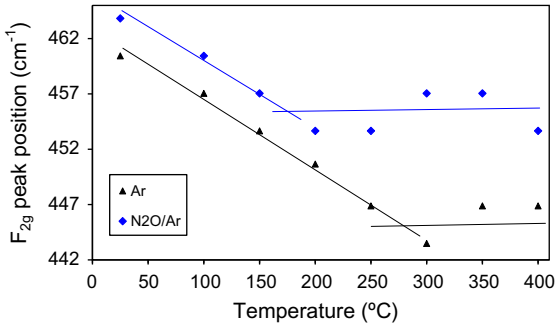

Fig. 5. Position of the F_{2g} ceria peak determined by Raman spectroscopy during *in situ* thermal treatments of the Rh/CeO_2 catalyst under Ar or 1000 ppm N_2O/Ar.

can be attributed to the expansion of the unit cell of ceria due to the partial reduction of Ce^{4+} cations (0.097 nm) to larger Ce^{3+} cations (0.114 nm). Once more, it is evidenced that the reduction occurred under inert gas is partially inhibited by N_2O, and the shift in the F_{2g} position is lower under N_2O/Ar than under pure Ar. These differences are mainly important above 250 °C, that is, once N_2O decomposition takes place (see Fig. 1b). This further evidences the active participation of the CeO_2 support in the N_2O decomposition mechanism over the Rh/CeO_2 catalyst.

3.4. Pulse experiments with isotopic gases ($^{15}N_2{}^{18}O$ and $^{18}O_2$)

In order to analyse the participation of the catalyst oxygen in the N_2O decomposition mechanism, pulse experiments have been performed with isotopic gases ($^{15}N_2{}^{18}O$ and $^{18}O_2$). Qualitative information could be obtained from the shape of the reactants ($^{15}N_2{}^{18}O$ and $^{18}O_2$) and products profiles, and as examples, the MS profiles monitored after $^{15}N_2{}^{18}O$ pulses to Rh/CeO_2 at 300 °C and 400 °C are included as Supplementary data (Fig. 4SM). These profiles revealed that there is no delay between the profiles of reactants and products, and neither delay with regard to reference Ar pulses. This means that the rates of all the oxygen exchange processes taking place upon $^{15}N_2{}^{18}O$ and $^{18}O_2$ pulses are much faster than the measuring time (1 s frequency; complete relaxation of the system takes about 80 s). This is consistent with previous $^{18}O_2$ pulse experiments performed with bare and La^{3+}-doped ceria in a TAP device, which operates in the milliseconds range of time, where delay in the products profiles with regard to $^{18}O_2$ and Ar pulses was neither observed [19,20].

3.4.1. $^{15}N_2{}^{18}O$ pulses

Fig. 6 presents results of $^{15}N_2{}^{18}O$ pulses over $Rh/\gamma\text{-}Al_2O_3$ and $\gamma\text{-}Al_2O_3$ (Fig. 6a) and over Rh/CeO_2 and CeO_2 (Fig. 6b). The $^{15}N_2{}^{18}O$, $^{15}N_2{}^{16}O$ and $^{15}N_2$ percentages in the gas mixture after the interaction with the solid bed have been plotted as a function of temperature. Additionally, ΣOxygen profiles have been also plotted, calculated as twice the sum of the percentage of the different O_2 species, that is:

$$\Sigma\text{Oxygen} : 2 \cdot (^{18}O_2 + {}^{18}O^{16}O + {}^{16}O_2)$$

Note that the ^{16}O atoms come from the solids ($Rh/\gamma\text{-}Al_2O_3$, $\gamma\text{-}Al_2O_3$, Rh/CeO_2 or CeO_2), while ^{18}O atoms come from the pulsed gas.

For $^{15}N_2{}^{18}O$ pulses, the processes that imply breaking and forming bonds could be the following: (i) oxygen exchange between $^{15}N_2{}^{18}O$ and solids, which would lead to $^{15}N_2{}^{16}O$ release and/or (ii) $^{15}N_2{}^{18}O$ decomposition with $^{15}N_2$ and O_2 release ($^{18}O_2$, $^{18}O^{16}O$

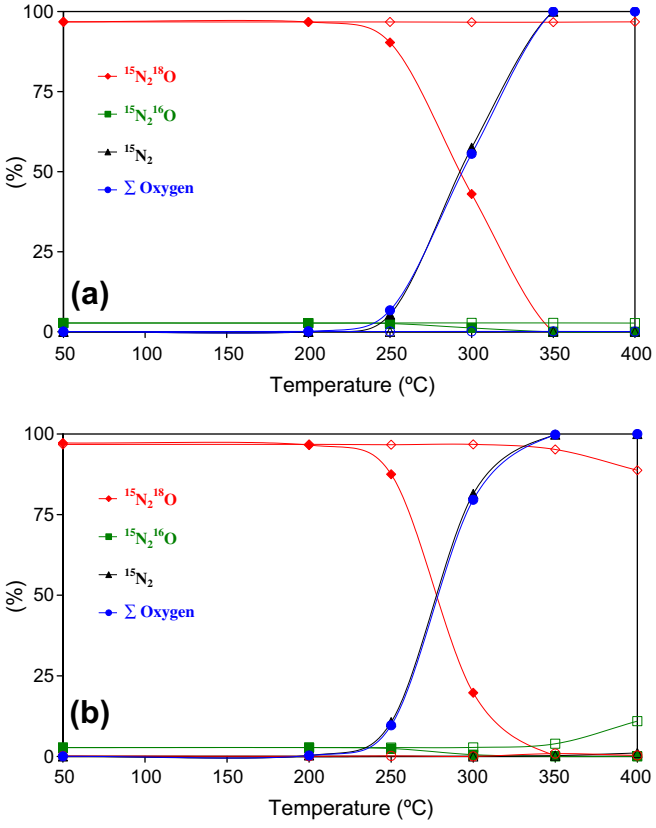

Fig. 6. $^{15}N_2{}^{18}O$ decomposition over (a) $Rh/\gamma\text{-}Al_2O_3$ and $\gamma\text{-}Al_2O_3$ (b) Rh/CeO_2 and CeO_2. Open symbols: supports; solid symbols: catalyst.

and/or $^{16}O_2$). The contribution of the former process is negligible in most cases and $^{15}N_2{}^{16}O$ formation is null in most pulse experiments, N_2O decomposition being the main process taking place. The CeO_2 support exchanges a very small amount of oxygen with the $^{15}N_2{}^{18}O$ gas leading to $^{15}N_2{}^{16}O$ release at 400 °C (Fig. 6b), but this phenomenon is not observed for γ-Al_2O_3 (Fig. 6a).

N_2O decomposition in the pulse experiments (Fig. 6) occurs above 250 °C with both catalysts. This temperature is quite consistent with the range of temperatures of N_2O decomposition in the conventional flow experiments (Fig. 1), in spite of the differences between both experimental procedures. The pulse experiments also reveal that the Rh/CeO_2 catalyst is more active for N_2O decomposition than Rh/γ-Al_2O_3 and that the supports have no activity for N_2O decomposition in the range of temperature studied in these experiments.

The stoichiometric formation of O_2 and N_2 from N_2O decomposition is observed in pulse experiments, since the ΣOxygen and $^{15}N_2$ percentage profiles overlap in Fig. 6. This means that the amount of nitrogen species stored on the catalysts during the N_2O decomposition process, which were identified by *in situ* DRIFTS experiments (see Figs. 9 and 10 and further discussion), is negligible with regard to the amount of N_2O pulsed and also that there is no appreciable oxygen accumulation on the catalysts under these experimental conditions.

Special attention must be paid to the nature of the O_2 molecules evolved as $^{15}N_2{}^{18}O$ decomposition product. In Fig. 7, the percentage of each O_2 species ($^{18}O_2$, $^{18}O^{16}O$ and $^{16}O_2$) with regard to the total O_2 has been plotted. Important differences in the O_2 species distribution are noticed between Rh/γ-Al_2O_3 (Fig. 7a) and Rh/CeO_2 (Fig. 7b). The most abundant O_2 species obtained with the Rh/γ-Al_2O_3 catalyst is $^{18}O_2$, which means that most of the O_2 delivered as N_2O decomposition product comes from the $^{15}N_2{}^{18}O$ molecules pulsed. The formation of $^{18}O^{16}O$ (and some $^{16}O_2$), which also occurs in a lower extent than $^{18}O_2$, implies a certain participation of the catalyst oxygen in the N_2O decomposition pathway. This will be discussed in detail afterwards.

The proportion of the different O_2 species evolved as $^{15}N_2{}^{18}O$ decomposition product significantly changes for Rh/CeO_2 (Fig. 7b). The main O_2 products are $^{16}O_2$ and $^{18}O^{16}O$, pointing out that the catalyst oxygen is actively involved in the N_2O decomposition mechanism as will be also discussed later.

3.4.2. $^{18}O_2$ pulses

Understanding the oxygen exchange between $^{18}O_2$ and the catalysts presents a double interest in the context of this study. On the one hand, O_2 released as N_2O decomposition product could interact again with the catalysts, and on the other hand, N_2O decomposition in O_2-rich streams has practical relevance.

The exchange of oxygen between the $^{18}O_2$ molecules and the catalysts can yield $^{18}O^{16}O$ and/or $^{16}O_2$. Fig. 8 shows the $^{18}O_2$, $^{16}O_2$ and $^{18}O^{16}O$ percentages upon $^{18}O_2$ pulses over Rh/γ-Al_2O_3 and γ-Al_2O_3 (Fig. 8a) and over Rh/CeO_2 and CeO_2 (Fig. 8b) at different temperatures. Oxygen exchange between the $^{18}O_2$ gas molecules pulsed and the supports is negligible in most experiments, but the presence of rhodium in the catalysts leads to the exchange of oxygen. With both catalysts, ^{16}O-containg O_2 molecules release above 200 °C, the oxygen exchange increasing with temperature. As expected, the phenomenon is much higher for Rh/CeO_2 compared to Rh/γ-Al_2O_3 [8–16,21,22].

For Rh/γ-Al_2O_3 (Fig. 8a), the main ^{16}O-containing product is $^{18}O^{16}O$. This indicates that the exchange of the oxygen atoms of the $^{18}O_2$ molecules pulsed occurs sequentially, and only single ex-

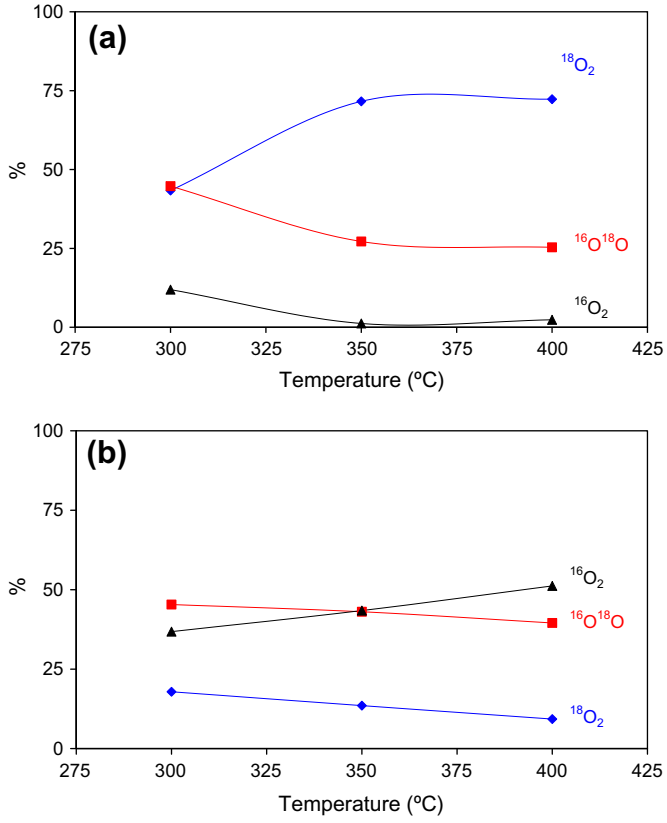

Fig. 7. Nature of the O_2 species evolved as $^{15}N_2{}^{18}O$ decomposition product with catalysts (a) Rh/γ-Al_2O_3 (b) Rh/CeO_2.

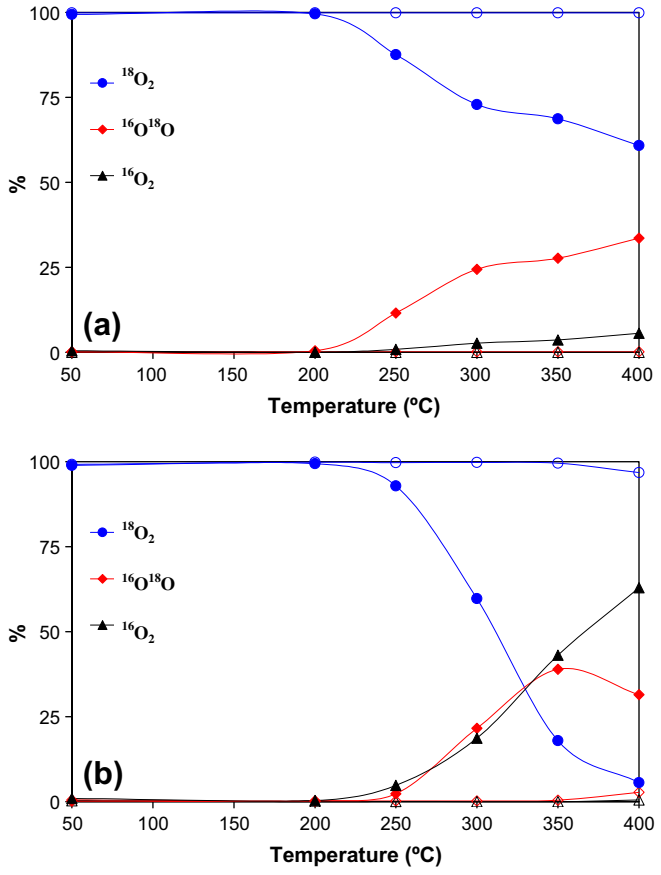

Fig. 8. Nature of the O_2 species evolved upon $^{18}O_2$ interaction with (a) Rh/γ-Al_2O_3 and γ-Al_2O_3 (b) Rh/CeO_2 and CeO_2. Open symbols: supports; solid symbols: catalyst.

change takes place under the experimental conditions used in these tests. Therefore, since re-adsorption of $^{16}O^{18}O$ upon $^{18}O_2$ pulses does not occur after the first oxygen exchange, the re-adsorption on Rh/γ-Al_2O_3 of O_2 molecules evolved as N_2O decomposition product is expected to be also minor under the experimental conditions of these pulse experiments.

On the contrary, both $^{16}O^{18}O$ and $^{16}O_2$ evolve above 200 °C after $^{18}O_2$ pulses over the Rh/CeO_2 catalyst (Fig. 8b). The $^{16}O^{18}O$ percentage reaches a maximum level at 350 °C, while the $^{16}O_2$ percentage rises monotonically with temperature. The formation of $^{16}O^{18}O$ evidences that single exchange of the $^{18}O_2$ oxygen atoms takes place. The formation of $^{16}O_2$ can occur by re-adsorption of $^{16}O^{18}O$ molecules and/or by double exchange of oxygen atoms once $^{18}O_2$ is adsorbed on the catalyst surface.

Finally, Table 4 shows the total amounts of ^{16}O atoms exchanged by the two catalysts during the pulse experiments, calculated on the basis of ^{16}O present in each catalyst as Rh_2O_3 or total (Rh_2O_3 + support oxygen). In the case of the Rh/CeO_2 catalyst, the amount of ^{16}O exchanged is much higher than the amount of oxygen on Rh_2O_3 (442%), confirming that oxygen atoms in CeO_2 are involved in the exchange processes. However, the amount of oxygen exchanged by Rh/CeO_2 with regard to the total amount of oxygen on this catalyst (Rh_2O_3 + CeO_2 oxygen) is very low (0.055%), pointing out that a large reservoir of non-exchanged oxygen remains on the catalyst after the pulse experiments. In the case of Rh/γ-Al_2O_3, the amount of oxygen exchanged only slightly exceeds the amount of Rh_2O_3 oxygen (145%). This confirms that the support γ-Al_2O_3 is only able to exchange a very little amount of oxygen with the isotopic gases, much less than CeO_2.

3.5. In situ DRIFTS-MS experiments

The surface of the catalysts has been studied under reaction conditions by DRIFT spectroscopy during *in situ* N_2O decomposition experiments. Figs. 9 and 10 show the DRIFT spectra recorded during these experiments. For the sake of brevity, the MS results recorded together with the spectra are not shown, but it has to be mentioned that the catalytic decomposition of N_2O in the DRIFTS cell occurs in the same range of temperatures observed in the flow reactor (Fig. 1) for both catalysts. The only difference between the results obtained in the flow reactor and in the DRIFTS cell is the N_2O decomposition rate reached at each temperature, which is lower in the DRIFTS cell due to gas diffusion effects. As an example, the MS profiles measured during the DRIFTS-MS experiment performed with Rh/γ-Al_2O_3 under 1000 ppm N_2O/He is presented as Supplementary data (Fig. 5SM).

Fig. 9 shows the DRIFT spectra recorded with the support γ-Al_2O_3 under N_2O and $N_2O + O_2$ (Fig. 9a and b, respectively), and their counterpart spectra recorded with the Rh/γ-Al_2O_3 catalyst under the same atmospheres (Fig. 9c and d, respectively). To clearly observe nitrogen-containing surface species, both on the support and on the catalyst, 200 °C or higher temperatures must be reached. The N–N stretching frequency of adsorbed N_2 or N_2O on metal oxides was reported to absorb within a wide range of frequencies, typically between 2400 and 2150 cm^{-1} [38–41]. In Fig. 9a–d, above 200 °C, a quite intense absorption band is observed at 2315 cm^{-1}, which could be assigned to adsorbed N_2O. Nitrites, nitrates and nitro compounds typically show bands below 1700 cm^{-1}. In all spectra of Fig. 9 recorded at temperatures higher than 200 °C, several peaks are identified below this wavenumber. The spectra of the γ-Al_2O_3 support and Rh/γ-Al_2O_3 catalyst under N_2O flow (Fig. 9a and c, respectively) are consistent with the formation of monodentate nitrites (bands in the range 1500–1400 cm^{-1}), monodentate nitrates (bands at 1570–1540 cm^{-1} and at 1290–1250 cm^{-1}) and/or nitro compounds (bands around 1345 cm^{-1}). The existence of nitrites, nitrates or nitro compounds in these spectra implies that the reaction between N_2O and oxygen at the support or catalyst surface is taking place.

In the presence of $N_2O + O_2$ (Fig. 9b and c), similar bands are observed, but the relative intensity of these bands is different from that measured under N_2O only. The formation of nitrates seems to be favoured at expenses of nitrites, that is, as expected, the surface species seems to be more oxidized under $N_2O + O_2$ than under N_2O.

As a main conclusion of the DRIFTS analysis presented in Fig. 9, it can be highlighted that the spectra of γ-Al_2O_3 (Fig. 9a and b), without catalytic activity in the temperature range studied, and of Rh/γ-Al_2O_3 (Fig. 9c and d), with catalytic activity, are quite similar. This suggests that most nitrogen species observed on the alumina samples upon N_2O exposure are not involved in the N_2O decomposition mechanism, but they seem to be just spectators, other way important differences between Rh/γ-Al_2O_3 and γ-Al_2O_3 would be expected. This also demonstrates that not all the adsorption sites suitable for N_2O adsorption are active for N_2O decomposition. The similarities between the Rh/γ-Al_2O_3 and γ-Al_2O_3 spectra also suggest that the surface nitrogen species are mainly created on the γ-Al_2O_3 support and not on rhodium.

This scenario significantly changes with the ceria samples. Fig. 10 shows the DRIFT spectra recorded with the CeO_2 support under N_2O and $N_2O + O_2$ (Fig. 10a and b, respectively) and their counterpart spectra recorded with the Rh/CeO_2 catalyst under the same atmospheres (Fig. 10c and d, respectively). As a general observation, the number of bands in the DRIFT spectra of Fig. 10 (ceria samples) is much higher than that in Fig. 9 (alumina samples), which evidences that the nature of nitrogen species created at the surface is more heterogeneous on ceria than on alumina.

Bands between 2390 and 2100 cm^{-1} appeared in the ceria samples above 200 °C, which could be assigned to the N–N stretching frequency of adsorbed N_2, produced as N_2O decomposition product, or of adsorbed N_2O [38–41]. The number of bands in this range of values is much higher in the ceria samples (Fig. 10a–d) than in those of alumina (Fig. 9a–d), which only showed a single band at 2315 cm^{-1}, evidencing the higher heterogeneity of the ceria surface. The appearance of several peaks in the Rh/CeO_2 catalysts, which did not appear in Rh/γ-Al_2O_3, should correspond to the existence of N_2 and/or N_2O adsorbed on different rhodium and/or cerium oxide sites.

The formation and transformation with temperature of absorption bands below 1700 cm^{-1} is very relevant in Fig. 10a–d. In bare CeO_2, below 200 °C, the absorption bands identified are consistent with the formation of monodentate nitrates both in the absence and presence of O_2 (Fig. 10a and b, respectively), with bands at 1560 and 1300 cm^{-1} which progress together. Above this temperature, these bands decrease and the spectra evidence the formation of some other nitrogen compounds. The bands at 1695 and 1230 cm^{-1} are consistent with the formation of bridged nitrates and those at 1530 and 1300 cm^{-1} with bidentate nitrates. Note that bridged and bidentate nitrates are more stable than monodentate nitrates, and therefore, they appear at higher temperatures. In addition, bands compatible with the formation of monodentate nitrites (1434 cm^{-1}) and nitro groups (1360 cm^{-1}) remain on bare CeO_2 between 200 and 350 °C. The formation of nitrites, nitrates

Table 4
Exchanged oxygen between gas molecules and catalysts in the pulse experiments performed with isotopic gases.

	Oxygen exchanged on Rh_2O_3 basis (%)	Oxygen exchanged on Rh_2O_3 + support basis (%)
Rh/γ-Al_2O_3	145	0.011
Rh/CeO_2	442	0.055

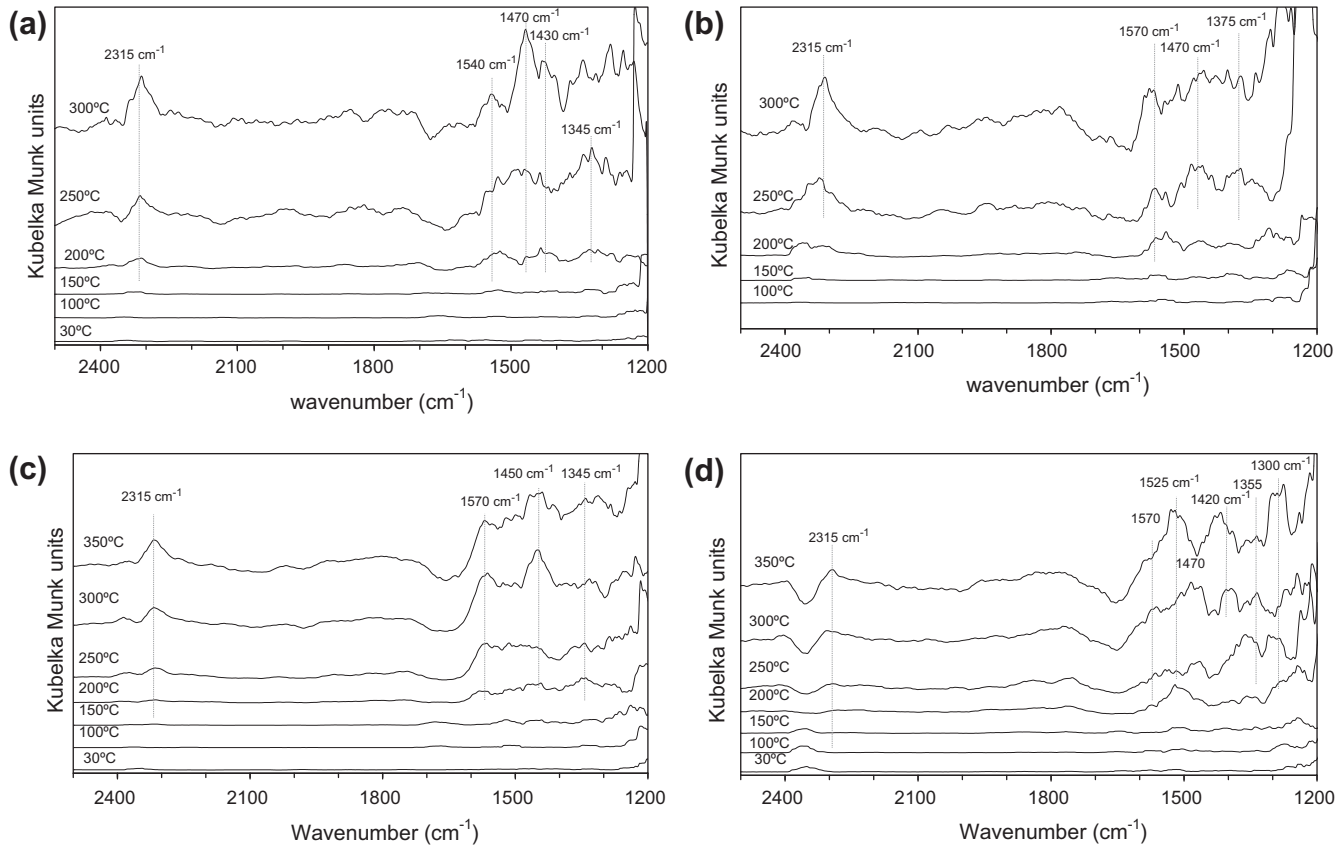

Fig. 9. *In situ* DRIFT spectra of: (a) γ-Al_2O_3 under N_2O, (b) γ-Al_2O_3 under $N_2O + O_2$, (c) Rh/γ-Al_2O_3 under N_2O, and (d) Rh/γ-Al_2O_3 under $N_2O + O_2$.

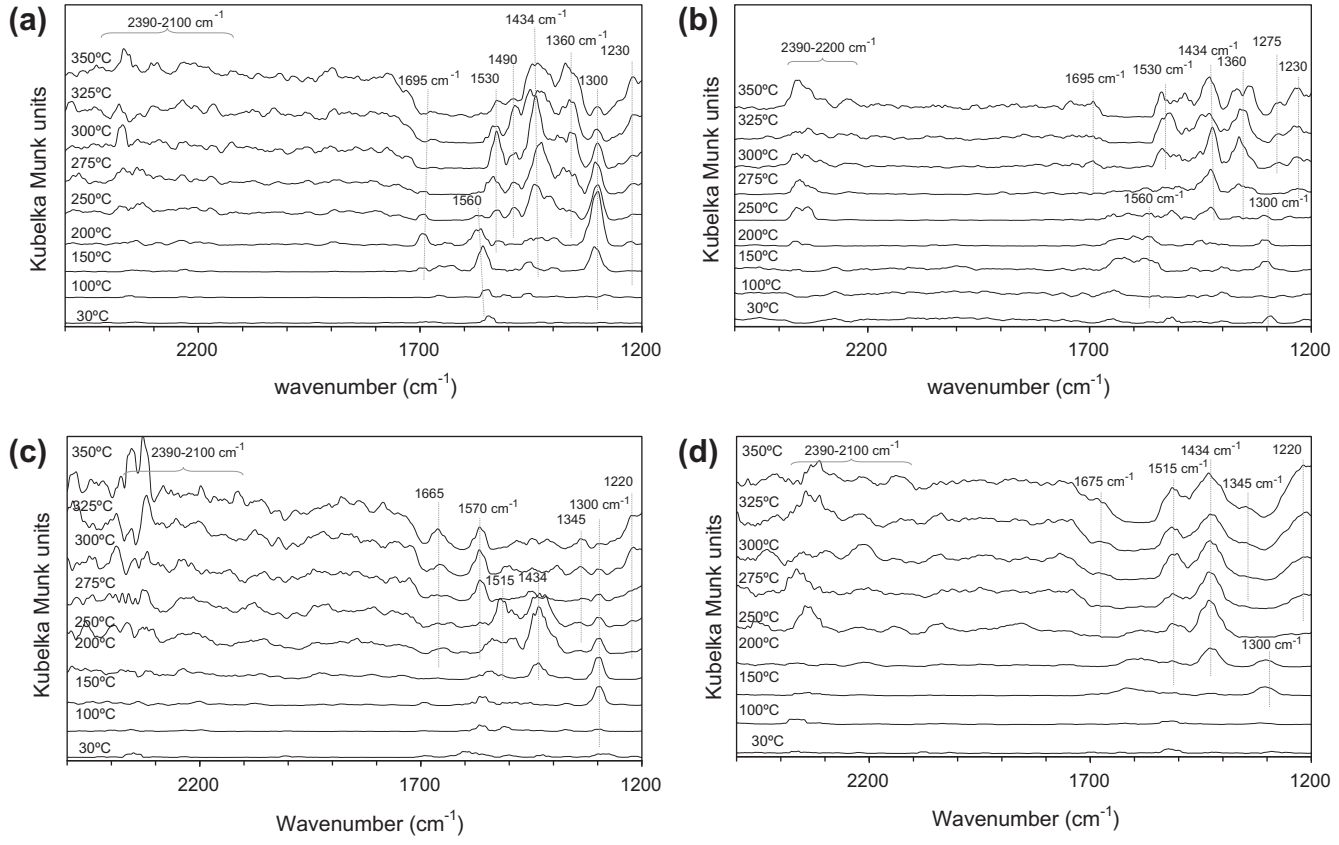

Fig. 10. *In situ* DRIFT spectra of: (a) CeO_2 under N_2O, (b) CeO_2 under $N_2O + O_2$, (c) Rh/CeO_2 under N_2O, and (d) Rh/CeO_2 under $N_2O + O_2$.

or nitro compounds in these spectra evidences the oxidation of N_2O with ceria oxygen. These complicated spectra compiled in Fig. 10a and b are in agreement with the previously commented heterogeneity of the ceria surface and evidence the high affinity of this metal oxide towards N_2O chemisorption and oxidation.

Below 200 °C, the nature of the surface species created on CeO_2 (Fig. 10a and b) seems to be quite similar to the nature of those created on Rh/CeO_2 (Fig. 10c and d) suggesting that, in the Rh/CeO_2 catalyst, these species are mainly created on ceria surface sites rather than on rhodium sites. However, the evolution with temperature of the surface species created on Rh/CeO_2 is very different to that observed on CeO_2, and this could be related to the catalytic activity of Rh/CeO_2 for N_2O decomposition. Under N_2O (Fig. 10c) and above 275 °C, that is, once N_2O is being decomposed on Rh/CeO_2, most bands in the range 1550–1200 cm^{-1} disappear. This means that monodentate nitrites and bidentate nitrates are not stable under reaction conditions. As it has been deduced from the pulse experiments with isotopic N_2O, ceria oxygen is involved in N_2O decomposition over Rh/CeO_2. This implies the constant creation of vacant sites on ceria, by oxygen depletion, and filling up such vacant sites by N_2O oxygen. The stabilization of certain nitrites and nitrates seems not to be possible under this dynamic behaviour of ceria oxygen. In the presence of O_2 (Fig. 10d), the depletion of surface nitrogen species under reaction conditions is slightly different than in the absence of O_2 (Fig. 10c). For instance, monodentate nitrites seem to remain stable during N_2O decomposition under $N_2O + O_2$ but not monodentate nitrates. This is consistent with the previous hypothesis, that is, under $N_2O + O_2$, O_2 keeps ceria more oxidized than under only N_2O, and then ceria is able to oxidize more easily the chemisorbed N_2O.

The main conclusion of this DRIFTS study is that both ceria and alumina chemisorb and oxidize N_2O, and the behaviour of the chemisorbed nitrogen species during N_2O decomposition on rhodium catalysts depends on the support nature. While the N_2O decomposition reaction over $Rh/\gamma\text{-}Al_2O_3$ does not affect the nitrogen surface species created on the $\gamma\text{-}Al_2O_3$ support, some of the oxidized nitrogen species created on ceria upon N_2O chemisorption (monodentate nitrites and bidentate nitrates, for instance) are not stable during N_2O decomposition. The reasons could be that the alumina support is not involved in the N_2O decomposition mechanism while ceria oxygen, which is required to oxidize N_2O, is involved in the N_2O decomposition process on ceria.

4. Discussion

The different techniques used in this study provide complementary information about the N_2O decomposition mechanisms catalysed by $Rh/\gamma\text{-}Al_2O_3$ and Rh/CeO_2, explaining why this catalyst is more active than the former one. As a main conclusion, it is demonstrated that the CeO_2 support, in the presence of Rh, is actively involved in the N_2O decomposition mechanism while $\gamma\text{-}Al_2O_3$ is not. The high catalytic activity for N_2O decomposition of RhO_x/CeO_2 catalysts was already reported, and it was proposed, based on ESR analysis, that the low-temperature activity of Rh/CeO_2 catalysts for N_2O decomposition relies on electron excess sites at microinterfaces between the dispersed rhodium component and the ceria support [42]. Further evidences about the synergy between rhodium and ceria in N_2O decomposition have been observed in this study.

Once the $Rh/\gamma\text{-}Al_2O_3$ and Rh/CeO_2 catalysts are put in contact with a N_2O stream surface nitrogen species are created on the supports, as demonstrated by the *in situ* DRIFTS experiments (See Figs. 9 and 10). This species include chemisorbed N_2O and oxidized nitrogen species like nitrites or nitrates. The oxidized nitrogen species are not reaction intermediates of the N_2O decomposition mechanisms, but they are just spectators. At 200 °C or higher temperatures, where N_2O decomposition into N_2 and O_2 takes place (see Fig. 1), these oxidized nitrogen species are stable on $Rh/\gamma\text{-}Al_2O_3$ while not all of them are stable on Rh/CeO_2, because the ceria oxygen required to oxidize N_2O is involved in the N_2O decomposition process.

From the pulse experiments performed with $^{15}N_2{}^{18}O$, it is deduced that several redox processes occur on the catalysts during N_2O decomposition. $^{15}N_2{}^{18}O$ decomposition on $Rh/\gamma\text{-}Al_2O_3$ yields $^{15}N_2 + {}^{18}O^{16}O$, and an oxidized rhodium site ($Rh*-{}^{16}O$) becomes reduced ($Rh*$) in this process:

$$Rh*-{}^{16}O + {}^{15}N_2{}^{18}O \rightarrow Rh* + {}^{15}N_2 + {}^{18}O^{16}O \quad \text{Step 1}$$

This reaction step explains the reduction of rhodium under reaction conditions, as deduced by XPS (Fig. 2a), and the $^{18}O^{16}O$ emission in pulse experiments (Fig. 7a). In the case of the $Rh/\gamma\text{-}Al_2O_3$ catalyst, the reoxidation of rhodium sites takes place with gas phase $^{15}N_2{}^{18}O$, as it is described by step 2:

$$Rh* + {}^{15}N_2{}^{18}O \rightarrow Rh*-{}^{18}O + {}^{15}N_2 \quad \text{Step 2}$$

Once the redox process described by steps 1 and 2 has occurred and part of the ^{16}O atoms (on Rh sites) have been removed, the decomposition of further $^{15}N_2{}^{18}O$ molecules yields $^{18}O_2$ instead of $^{18}O^{16}O$, since the oxidized rhodium sites are progressively occupied by ^{18}O atoms, that is:

$$Rh*-{}^{18}O + {}^{15}N_2{}^{18}O \rightarrow Rh* + {}^{15}N_2 + {}^{18}O_2 \quad \text{Step 1bis}$$

This explains why $^{18}O_2$ is the main molecular oxygen species yielded in $Rh/\gamma\text{-}Al_2O_3$-catalysed N_2O decomposition (Fig. 7a).

The formation of $^{16}O_2$, which is minor when $^{15}N_2{}^{18}O$ is decomposed on the $Rh/\gamma\text{-}Al_2O_3$ catalyst (Fig. 7a), would occur by recombination of two ^{16}O-containing oxidized rhodium sites:

$$2Rh*-{}^{16}O \rightarrow 2Rh* + {}^{16}O_2 \quad \text{Step 3}$$

The preferential formation of $^{18}O^{16}O$ (step 1) with regard to $^{16}O_2$ (step 3) by the $Rh/\gamma\text{-}Al_2O_3$ catalyst (Fig. 7a) evidences that the Eley–Rideal mechanism (reduction of the noble metal sites by N_2O; step 1) is the main reaction pathway while the Langmuir–Hinshelwood mechanism (recombination of two oxygen atoms on noble metal sites yielding molecular oxygen; step 3) has a marginal contribution. The active sites for $Rh/\gamma\text{-}Al_2O_3$ catalyst ($Rh*$) could be ascribed to Rh^0.

The N_2O decomposition mechanism described by steps 1, 1bis and 2 is valid for the $Rh/\gamma\text{-}Al_2O_3$ catalyst, but the reaction pathway is much more complicated on Rh/CeO_2, since the steps 1, 1bis and 2 are not able to explain the high proportion of $^{16}O_2$ yielded by this catalyst (Fig. 7b). The *in situ* XPS experiments (Fig. 2) demonstrate that ceria stabilizes the cationic species of rhodium during N_2O decomposition, while rhodium on $Rh/\gamma\text{-}Al_2O_3$ is reduced to Rh^0. Therefore, the sequence of steps 1, 1bis and 2 seems to occur preferentially on reduced rhodium, being the main reaction pathway for $Rh/\gamma\text{-}Al_2O_3$ and having a minor contribution for Rh/CeO_2.

The participation of ceria oxygen in the N_2O decomposition mechanism over Rh/CeO_2 is supported by the fact that the amount of ^{16}O atoms released during the pulse experiments with isotopic gases is much higher than the amount of oxygen on Rh_2O_3 (see Table 4). Taking the XPS results into account, the participation of the support could consist of oxygen transfer from ceria to rhodium (step 4), that is, once N_2O reduces a rhodium site via step 1, the reoxidation of this site could be accomplished by ceria oxygen:

$$Rh* + Ce*-{}^{16}O \rightarrow Rh*-{}^{16}O + Ce* \quad \text{Step 4}$$

Probably this oxygen transfer is related to the high dispersion of Rh observed on CeO_2. In the case of Rh/CeO_2 catalyst, the active site for rhodium ($Rh*$) not necessarily means Rh^0, but RhO_x species at the Rh–ceria interface, as proposed by Cunningham et al. [42].

The transfer of oxygen from ceria to the rhodium site leads to the creation of vacant sites on the ceria support (Ce∗), and ceria must restore the oxygen balance re-oxidizing such vacant sites by $^{15}N_2{}^{18}O$:

$$Ce* + {}^{15}N_2{}^{18}O \rightarrow Ce* - {}^{18}O + {}^{15}N_2 \quad \text{Step 5}$$

The constant Ce^{3+} percentages estimated by XPS (Fig. 3) on Rh/CeO_2 after *in situ* N_2O decomposition treatments supports that the step 5 takes place, that is, the XPS experiments demonstrate that the ceria vacant sites can be reoxidized by N_2O. Additional experimental evidence supporting the participation of step 5 is obtained by *in situ* Raman spectroscopy experiments (Fig. 5). These experiments demonstrated that the thermal expansion of the ceria lattice, due to the partial reduction of Ce^{4+} cations to Ce^{3+}, is hindered by reoxidation of these Ce^{3+} cations in the presence of N_2O.

The sequence of steps 1 + 4 + 5 can explain the emission of $^{18}O^{16}O$ by the Rh/CeO_2 catalyst upon $^{15}N_2{}^{18}O$ decomposition (Fig. 7b). Additionally, the high proportion of $^{16}O_2$ yielded by this catalyst could be mainly attributed to the recombination of oxygen atoms on two oxidized sites. These oxidized sites could be two rhodium sites (step 3), two cerium sites (step 6) or a rhodium site and a cerium site (step 7):

$$2Ce* - {}^{16}O \rightarrow 2Ce* + {}^{16}O_2 \quad \text{Step 6}$$

$$Rh* - {}^{16}O + Ce* - {}^{16}O \rightarrow Rh* + Ce* + {}^{16}O_2 \quad \text{Step 7}$$

Taking the described mechanisms and the different experimental observations into account, it can be concluded that Rh^0 are the most active sites for N_2O decomposition on Rh/γ-Al_2O_3, while the opposite occurs on the Rh/CeO_2 catalyst. Despite Rh^0 percentage increases on Rh/CeO_2 with temperature (Table 3), the highest activity is expected to remain on RhO_x sites with high contact with ceria [42]. The experimental evidence to support this is the participation of ceria oxygen in the N_2O decomposition mechanism, deduced from isotopic exchange experiments, even at temperatures where Rh^0 percentage is higher than that of Rh^{3+} (275 °C and higher temperature, Table 3). The $^{15}N_2{}^{18}O$ decomposition mechanism occurring exclusively on Rh^0 sites, without ceria oxygen participation, would yield $^{18}O_2$ (mechanism described by steps 2 and 1b). However, $^{16}O_2$ and $^{16}O^{18}O$ are the main O_2 species evolved above 275 °C upon N_2O decomposition on the Rh/CeO_2 catalysts (Fig. 7b), and this means that most N_2O is decomposed throughout a mechanism that involves steps 4–7. In this reaction pathway, step 4 is responsible to keep rhodium sites partially oxidized under reaction conditions.

In conclusion, several N_2O decomposition mechanisms seem to occur concomitantly on Rh/CeO_2, and all the processes described by steps 1–7 participate in the N_2O decomposition pathways. These reaction mechanisms occurring on Rh/CeO_2 are more effective than those based exclusively on steps 1, 1bis and 2 (occurring on Rh/γ-Al_2O_3), because the active sites for N_2O chemisorption and decomposition are not only located on rhodium but also on ceria.

5. Conclusions

The study of the N_2O decomposition on Rh/γ-Al_2O_3 and Rh/CeO_2 allows concluding that:

- The Rh/γ-Al_2O_3 catalyst is less active for N_2O decomposition than Rh/CeO_2, and the apparent activation energies (146 and 121 kJ/mol, respectively) are consistent with such differences in activity. The different activity is related to the fact that the CeO_2 support is actively involved in the N_2O decomposition mechanism while γ-Al_2O_3 is not.
- The ceria support strongly interacts with rhodium and stabilizes oxidized species of the noble metal of very small particle size during N_2O decomposition, while rhodium on Rh/γ-Al_2O_3 is reduced to Rh^0 under reaction conditions.
- N_2O decomposition over Rh/γ-Al_2O_3 mainly occurs via the Eley–Rideal mechanism (successive oxidation and reduction of the noble metal sites by N_2O) while the Langmuir–Hinshelwood mechanism (oxidation of the noble metal sites by N_2O and recombination of two oxygen atoms on noble metal sites yielding molecular oxygen) has a marginal contribution.
- In Rh/CeO_2, once N_2O reduces a rhodium site this site can be reoxidized either by another N_2O molecule or by ceria oxygen. In the latter case, N_2O subsequently oxidizes the vacant site created on ceria.
- In Rh/CeO_2, the active sites for N_2O chemisorption and decomposition are not only placed on rhodium but also on ceria.

Acknowledgment

The authors thank the financial support of the Spanish Ministry of Science and Innovation, Project CIT-420000-2009-48, partially funded with FEDER resources.

Appendix A. Supplementary material

Supplementary data associated with this article can be found, in the online version, at doi:10.1016/j.jcat.2010.10.001.

References

[1] F. Kapteijn, J. Rodríguez-Mirasol, J.A. Moulijn, Appl. Catal. B. 9 (1996) 25.
[2] J.C. Groen, J.C. Jansen, J.A. Moulijn, J. Pérez-Ramírez, J. Phys. Chem. B 108 (2004) 13062.
[3] V.A. Kondratenko, M. Baerns, J. Catal. 225 (2004) 37.
[4] E.V. Kondratenko, J. Pérez-Ramirez, Catal. Lett. 91 (2003) 211.
[5] S. Tanaka, K. Yuzaki, S. Ito, H. Uetsuka, S. Kameoka, K. Kunimori, Catal. Today 63 (2000) 413.
[6] T.M. Miller, V.H. Grassian, J. Am. Chem. Soc. 117 (1995) 10969.
[7] H. Kobayashi, M. Kobayashi, Catal. Rev. Sci. Eng. 10 (1974) 139.
[8] A. Bueno-López, K. Krishna, B. van der Linden, G. Mul, J.A. Moulijn, M. Makkee, Catal. Today 121 (2007) 237.
[9] H. He, H.X. Dai, K.W. Wong, C.T. Au, Appl. Catal. A 251 (2003) 61.
[10] D. Martin, P. Kaur, D. Duprez, E. Gaigneaux, P. Ruiz, B. Delmon, Catal. Today 32 (1996) 329.
[11] Y. Madier, C. Descorme, A.M. Le Govic, D. Duprez, J. Phys. Chem. B 103 (1999) 10999.
[12] A. Holmgren, B. Andersson, J. Catal. 178 (1998) 14.
[13] A. Holmgren, D. Duprez, B. Andersson, J. Catal. 182 (1999) 441.
[14] J. Novakova, Catal. Rev. 4 (1970) 77.
[15] K. Klier, J. Nováková, P. Jíru, J. Catal. 2 (1963) 479.
[16] S. Parres-Esclapez, M.J. Illán-Gómez, C. Salinas-Martínez de Lecea, A. Bueno-López, Appl. Catal. B 96 (2010) 370.
[17] A. Bueno-López, I. Such-Basáñez, C. Salinas-Martínez de Lecea, J. Catal. 244 (2006) 102.
[18] J. Cunningham, F. Farrell, C. Gibson, J. McCarthy, Catal. Today 50 (1999) 429.
[19] A. Bueno-López, K. Krishna, M. Makkee, J.A. Moulijn, J. Catal. 230 (2005) 237.
[20] A. Bueno-López, K. Krishna, M. Makkee, J.A. Moulijn, Catal. Lett. 99 (2005) 203.
[21] A. Holmgren, B. Andersson, D. Duprez, Appl. Catal. B 22 (1999) 215.
[22] A. Bueno-López, K. Krishna, M. Makkee, Appl. Catal. A 342 (2008) 144.
[23] J. Oi, A. Obuchi, G.R. Bamwenda, A. Ogata, H. Yagita, S. Kushiyama, K. Mizuno, Appl. Catal. B 12 (1997) 277.
[24] K. Yuzaki, T. Yarimizu, K. Aoyagi, S.-i. Ito, K. Kunimori, Catal. Today 45 (1998) 129.
[25] K. Jones, J.C. Bailar, H.J. Emeleus, R. Nyholm, A.F. Trotman-Dickenson (Eds.), Comprehensive Inorganic Chemistry, Pergamon Press, Oxford, 1984, pp. 316–323.
[26] N.N. Greenwood, A. Eamshaw, Chemistry of the Elements, Pergamon Press, Oxford, 1984.
[27] W.M. Kalback, C.M. Sliepcevich, Ind. Eng. Chem. Fundam. 17 (1978) 165.
[28] B.G. Reuben, J.W. Linnett, Trans. Faraday Soc. 55 (1959) 1543.
[29] O.R. Wulf, J. Am. Chem. Soc. 54 (1932) 833.
[30] J. Kaspar, P. Fornasiero, M. Graziani, Catal. Today 50 (1999) 285.
[31] J. Soria, A. Martinez-Arias, J.L. García-Fierro, J.C. Conesa, Vacuum 46 (1995) 1201.
[32] http://www.lasurface.com/.
[33] I. Cuauhtémoc, G. Del Angel, G. Torres, V. Bertin, Catal. Today 133–135 (2008) 588.

[34] A. Laachir, V. Perrichon, A. Badri, J. Lamotte, E. Catherine, J.C. Lavalley, J. El Fallal, L. Hilaire, F. le Normand, E. Quéméré, G.N. Sauvion, O. Touret, J. Chem. Soc. Faraday Trans. 87 (1991) 1601.
[35] S. Music, A. Saric, S. Popovic, M. Ivanda, J. Mol. Struct. 924–926 (2009) 221.
[36] V.V. Pushkarev, V.I. Kovalchuk, J.L. d'Itri, J. Phys. Chem. B 108 (2004) 5341.
[37] A. Nakajima, A. Yoshihara, M. Ishigame, Phys. Rev. B 50 (1994) 13297.
[38] K.I. Hadjiivanov, Catal. Rev. Sci. Eng. 42 (2000) 71.
[39] N. Oktar, J. Mitome, E.M. Holmgreen, U.S. Ozkan, J. Mol. Catal. A. 259 (2006) 171.
[40] Y. Wang, Z. Lei, B. Chen, Q. Guo, N. Liu, Appl. Surf. Sci. 256 (2010) 4042.
[41] S. Haq, A. Hodgson, Surf. Sci. 463 (2000) 1.
[42] J. Cunningham, J.N. Hickey, R. Cataluna, J.C. Conesa, J. Soria, A. Martinez-Arias, Stud. Surf. Sci. Catal. 101 (1996) 681.